

Numerical modeling and global performance analysis of a 15-MW Semisubmersible Floating Offshore Wind Turbine (FOWT)

Da Li¹, Ikjae Lee², Cong Yi¹, Wei Gao¹, Chunhui Song¹, Shenglei Fu¹,
Moohyun Kim^{*2}, Alex Ran³ and Tuanjie Liu³

¹CNOOC Ltd, No. 6 Taiyanggong South Avenue, Chaoyang District, Beijing 100028, China

²Department of Ocean Engineering, Texas A&M University, College Station, Texas 77843, USA

³OffshoreTech, LLC 1400 Broadfield Blvd, Suite 625, Houston, TX 77084, USA

(Received August 10, 2023, Revised September 2, 2023, Accepted September 15, 2023)

Abstract. The global performance of a 15 MW floating offshore wind turbine, a newly designed semi-submersible floating foundation with multiple heave plates by CNOOC, is investigated with two independent turbine-floater-mooring coupled dynamic analysis programs CHARM3D-FAST and OrcaFlex. The semisubmersible platform hosts IEA 15 MW reference wind turbine modulated for VoltornUS-S and hybrid type (chain-wire-chain with clumps) 3x2 mooring lines targeting the water depth of 100 m. The numerical free-decay simulation results are compared with physical experiments with 1:64 scaled model in 3D wave basin, from which appropriate drag coefficients for heave plates were estimated. The tuned numerical simulation tools were then used for the feasibility and global performance analysis of the FOWT considering the 50-yr-storm condition and maximum operational condition. The effect of tower flexibility was investigated by comparing tower-base fore-aft bending moment and nacelle translational accelerations. It is found that the tower-base bending moment and nacelle accelerations can be appreciably increased due to the tower flexibility.

Keywords: 15 MW semi-submersible floating foundation; flexible vs rigid tower; free-decay simulation/experiment; fully coupled dynamics simulation; heave damping plates

1. Introduction

Offshore wind is the fastest growing clean and renewable energy resource. The fixed-type offshore wind turbines made substantial contributions to the wind energy production but they are constrained by depth limitations (e.g., less than 50 m). Floating Offshore Wind Turbines (FOWTs), on the other hand, have the potential to harness more reliable offshore wind energy in deeper waters where wind speeds are higher and more consistent. Moreover, wind farms in deeper waters are generally less sensitive to space availability, noise/visual restriction, resident opposition, and regulatory problems.

Design specifics of existing and planned FOWTs are not open to the public, which poses a barrier to collaboration on research and further development (Wu and Kim 2021). To promote collaboration, many institutions across the world have built reference wind turbine models with the floating structures which are publicly available for use (Jonkman *et al.* 2009, Bak *et al.* 2013, Gaertner *et al.*

*Corresponding author, Professor, E-mail: m-kim3@tamu.edu

2020). Representatively, the National Renewable Energy Laboratory (NREL) has published the definition of reference 5MW wind turbine with the corresponding OC4 semi-submersible design (Robertson *et al.* 2014a). More recently, NREL published a 15 MW reference offshore wind turbine model accompanied by semisubmersible type floating structure design called “UMaine VoltturnUS-S” (Allen *et al.* 2020). In parallel with this development, EU horizon 2020 project COREWIND (COst Reduction and increase performance of floating WIND technology) has also developed two concrete-material floating structures, semisubmersible-type “Activefloat” and spar-type “WindCrete”, being able to support the IEA 15 MW reference offshore wind turbine (Mahfouz *et al.* 2021). The reference models have been widely used for various purposes including (a) code-to-code comparison for coupled aero-hydro-servo-elastic-mooring dynamic analysis programs (Robertson *et al.* 2014b, Rinker *et al.* 2020, Chen *et al.* 2023), (b) improvement of numerical modeling practices (Wang *et al.* 2022), (c) Scaling and variation of reference models to develop new designs (Kikuchi *et al.* 2019; Wu and Kim 2021, Abdelmoteleb *et al.* 2022), and (d) Application of new floating bases to the reference wind turbine models (Jonkman and Matha 2011, Xue 2016, Tian 2016, Islam 2016).

Among various types of floating offshore wind turbine platforms, semisubmersible is gaining high attention in recent years. The semi-submersible floating structure is usually composed of several large columns connected by slender bracings (Gomes *et al.* 2022). The semisubmersible type platforms can take advantages of quay-side-assembly capability and wet towing due to its excellent stability. Recently, it has been successfully implemented in the world’s second floating wind farm – WindFloat Atlantic in Portugal which consists of three 8.4MW WindFloat semisubmersibles (EDP renewable 2020, Xu *et al.* 2021).

In conjunction with FOWT development, the use of heave plates is an important design consideration. The heave plates can significantly reduce heave-roll-pitch floater motions. Heave plates are strategically placed at the bottom of columns or pontoons so that it provides damping at minimal wave-induced forces. Lopez-Pavon and Souto-Iglesias (2015) carried out an experimental study to evaluate the performance of the heave plates in semisubmersible platform and have observed that damping and added mass coefficients have weak dependence with frequency but have large dependence with motion amplitude. Jang *et al.* (2019) investigated the effects of heave plates in a semisubmersible-type MUFOWT (Multi-Unit Floating Offshore Wind Turbine) and observed significant reductions in heave and pitch motions.

Typical mooring systems for semisubmersible FOWTs are composed of catenary chain or wire and their weights enable the platform to maintain its position within the limited offset. However, this concept is particularly difficult and challenging in shallow water regions where the effective water depth from fairlead to seabed becomes limited to secure sufficient pretension and geometric stiffness (Huang and Yang 2021). In this regard, heavy clumps are employed in the present study near the touchdown zone of the mooring lines. However, in extreme conditions, the clump weight may be lifted from the seabed to establish a temporarily stiffer mooring system to minimize the floater motion (Xu *et al.* 2021).

The global performance analysis of FOWTs can be conducted by aero-hydro-servo-elastic-mooring coupled dynamics simulation program like OpenFAST (NREL 2023), OrcaFlex (Orcina 2023), and CHARM3D-FAST (TAMU e.g., Bae and Kim 2011, 2014). The CHARM3D-FAST program is the combination of TAMU-CHARM3D (e.g., Arcandra and Kim 2003, Yang and Kim 2010) and NREL-FAST (Jonkman, 2005). In the program FAST, the rotor aerodynamics is solved by AeroDyn sub-module (Moriarty and Hansen 2005) with inflow wind files including binary type full-field turbulence generated by TurbSim (Jonkman 2009), and the servo-dynamics by ROSCO (Reference Open-Source COntroller) where collective blade-pitch and generator torque controllers

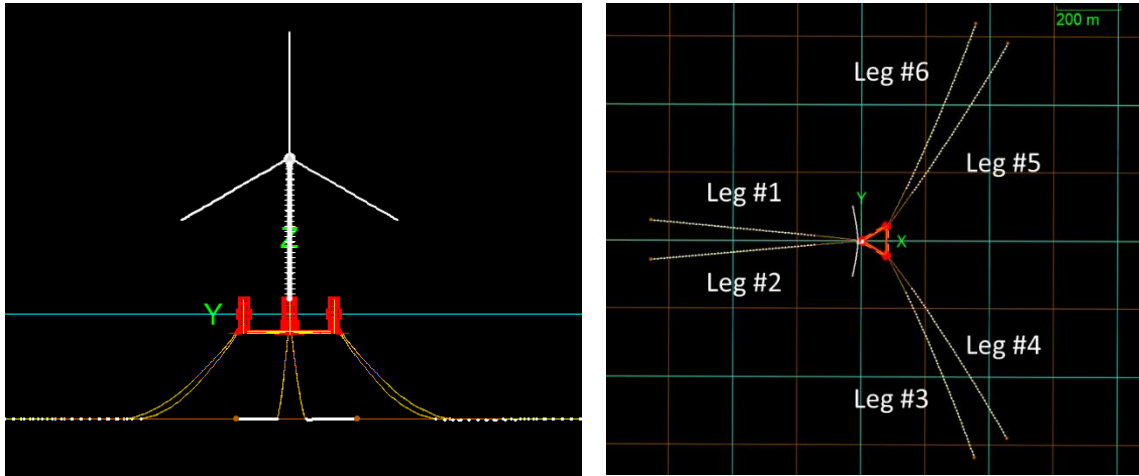


Fig. 1 15 MW-CNOOC semisubmersible FOWT: (left) front view, (right) bird-eye view

are used based on control parameters pre-tuned by ROSCO toolbox (Abbas *et al.* 2021). In the program CHARM3D, the time-domain hydrodynamics of the platform is solved using the Cummins' equation (Cummins 1962) and the mooring line dynamics is solved based on high-order FE-based rod theory (Garrett 1982, Ran 2000). The CHARM3D-FAST has been applied to various types of FOWTs including mini-TLP, Hywind spar, OC4 semisubmersible, and KRISO MUFOWT and validated against various scaled physical tests (e.g., Kim and Kim 2016, Kim *et al.* 2017, Jang *et al.* 2019).

In this study, we examined the feasibility and global performance of a 15MW semisubmersible CNOOC FOWT with multiple heave plates at water depth of 100m by using the CHARM3D-FAST program. Model descriptions and system particulars of the 15 MW semisubmersible FOWT are detailed in section 2. In section 3, its numerical modeling is described including the comparison with free-decay model test result. Lastly, numerical simulation results and analyses are given for various cases in section 4, which is followed by concluding remarks in section 5.

2. Model descriptions and system particulars

Fig. 1 shows the 15 MW CNOOC semisubmersible FOWT, which is investigated in this paper. The FOWT consists of IEA 15MW reference wind turbine, 3-column semisubmersible floating foundation and six (3×2) chain-steel wire-chain catenary mooring lines. The target water depth of the present study is 100m. Fig. 1 shows the global front and bird-eye views of CNOOC semisubmersible FOWT and its mooring lines. More details for each system component are described in Table 1.

2.1 IEA 15 MW reference offshore wind turbine

The IEA 15MW offshore reference wind turbine (Gaertner 2020) was also used in VoltturnUS semisubmersible FOWT models (Allen *et al.* 2020). In this study, the IEA 15MW offshore reference

Total System Particulars

Table 1 Specification of IEA 15MW wind turbine (UMaine VoltturnUS-S) with CNOOC semisubmersible platform

Parts	Parameter	Units	Value
15MW turbine (RNA + tower)	Power Rating	MW	15.0
	Rotor Radius	m	120.0
	Blade Length	m	117.0
	Hub Radius	m	3.0
	Hub Height	m	150.0
	RNA Mass	t	991
	RNA VCG above MWL	m	150.0
	Tower Base Diameter	m	10.0
	Tower Top Diameter	m	6.5
	Tower Length	m	144.6
	Tower Mass	t	1263
	Tower VCG above MWL	m	69.0
CNOOC semi- submersible platform	Spacing b/w column centers	m	86
	Draft below MWL	m	18
	Main column (diameter x height)	m	15 × 20 (upper part) 17 × 13 (lower part)
	Side column (diameter x height)	m	11 × 10 (upper part) 15 × 10 (sleeve part) 11 × 13 (lower part)
	Pontoon (length x width x height)	m	74 × 6 × 3 (main-side) 72 × 6 × 3 (side-side)
	Circular heave plate (diameter x height)	m	28 × 0.3
	Rectangular heave plate (length x width x height)	m	21 × 4 × 0.3
	Platform Mass	t	9.8E+03
	Platform raii of gyration (R_{xx}, R_{yy}, R_{zz})	m	(35, 40, 44)
	Platform center of mass (x_G, y_G, z_G)	m	(53, 0, -9.3)

wind turbine model modulated for the VoltturnUS-S is used (Lee and Kim 2022). In Table 1, the system particulars for the entire IEA reference turbine are given. The total mass including floater, tower, and RNA is 12.05 kton.

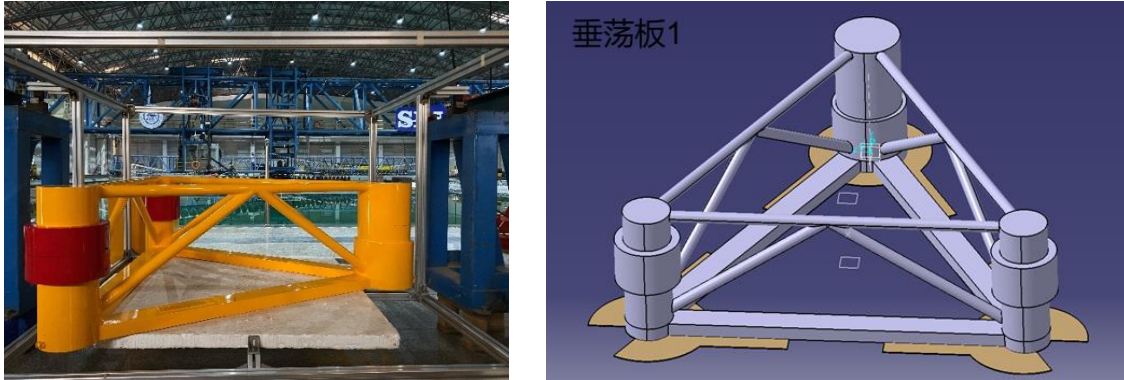


Fig. 2 CNOOC semisubmersible hull without (left) and with (right) heave plates

Table 2 Fairlead and anchor Locations (Unit: m)

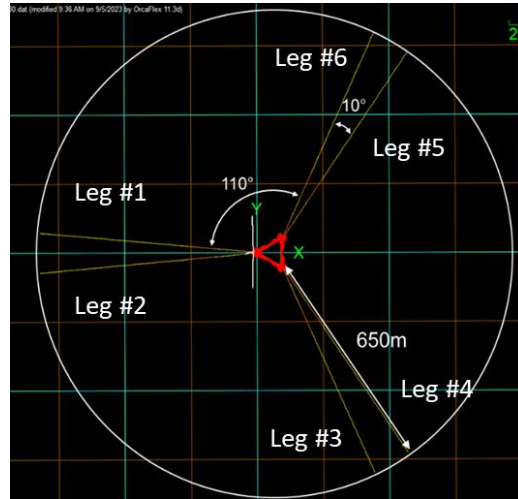
Line #	Fairlead Location			Anchor Location		
	X	Y	Z	X	Y	Water Depth
L1	-8.28	1.52	-16.5	-655.81	58.17	100
L2	-8.28	-1.52	-16.5	-655.81	-58.17	100
L3	80.00	-49.45	-16.5	354.71	-638.55	100
L4	82.55	-47.80	-16.5	455.38	-580.25	100
L5	82.55	47.80	-16.5	455.38	580.25	100
L6	80.00	49.45	-16.5	354.71	638.55	100

2.2 CNOOC Semi-submersible platform

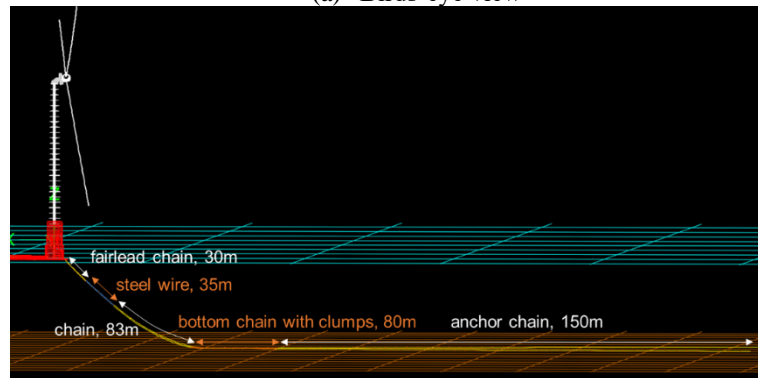
As shown in Fig. 2, 3-column semisubmersible platform is designed by CNOOC. The geometry is characterized by non-equal-sized main and side columns and large heave damping plates. The coordinate origin is located at MWL and aligned with the main column where the 15 MW offshore wind turbine is to be placed on. The heave plates are indented to increase heave and pitch damping (see Fig. 3).

2.3 Mooring system

Fig. 3 shows bird-eye and side views of the designed mooring system and line components at target water depth of 100m. The mooring system consist of 3×2 lines, and all legs have the equal size with chain-wire-chain and clumps. Fairlead and anchor locations are given in Table 3 and the mooring components for each leg are detailed in Table 4. Since the considered target water depth is relatively shallow (100 m), it is difficult to have high pre-tensions due to insufficient suspended length. Therefore, in such a case, it is normal to increase the size, accordingly the weight, of the chain, which results in significant increase of cost. Rather, the present mooring system takes advantage of the clumps which is attached to the bottom chain near touch-down point, as shown in Fig. 3(b).



(a) Birds-eye view



(b) side view (Leg #1)

Fig. 3 Mooring system details

Table 3 Mooring line components

Type	Units	Fairlead Chain	Steel wire	Bottom Chain	Bottom Chain with clumps	Anchor Chain
Diameter	mm	152	131	152	152	152
Breaking Strength	kN	18318	16775	18318	18318	18318
(Corroded)		(16388)		(16388)	(16388)	(16388)
Axial Stiffness	MN	1973	1552	1973	1973	1973
Dry Weight	kg/m	506	89.3	506	2000	506
Wet Weight	kg/m	440	68.7	440	1934	440
Length	m	30	35	83	80	150

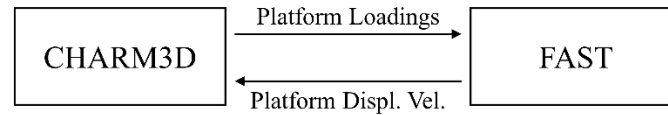


Fig. 4 Basic concept of CHARM3D-FAST coupling

Table 4 Numerical modeling of added mass/drag/spring coefficients for mooring system

Components	Parameters	Unit	Value
R3S Chain	Normal added mass coefficient	-	1.0
	Normal drag coefficient	-	2.4
Steel wire	Normal added mass coefficient	-	1.0
	Normal drag coefficient	-	1.2
Seabed	Normal quadratic spring stiffness	kN/m ² /m	100.0

3. Numerical modeling

3.1 CHARM3D-FAST (in-house computer program)

For turbine-floater-mooring coupled dynamic simulation and analysis, CHARM3D-FAST program is used. Specifically, the aero-servo-elasto-dynamic analysis program FAST (version 7) by NREL is coupled with floater-mooring coupled dynamic analysis program CHARM3D, which has been developed for more than 30 years by Prof. Kim's lab at TAMU and widely adopted for the coupled dynamic analysis of various offshore structures in the offshore industry. The CHARM3D-FAST program has analyzed various types of FOWTs (e.g., Shim and Kim 2007, Bae and Kim 2017) including 5 MW NREL semisubmersible (Kim and Kim 2016, 2017), 5 MW Hywind Spar (Bae and Kim 2014), and KRISO multi-unit FOWTs (Jang et al., 2019) and so on and they have been validated by the corresponding experiments (e.g., Kim *et al.* 2016, 2017, Jang *et al.* 2019). The basic concept of CHARM3D-FAST coupling is schematically shown in Fig. 4. In principle, the CHARM3D-FAST is similar to NREL's open-source program OpenFAST. However, in the hull hydrodynamics model of OpenFAST program, HydroDyn, the Morison forces used to be applied at the mean position. On the other hand, in the CHARM3D-FAST, the Morison force is applied at hull's instantaneous position and up to the instantaneous free-surface elevation, which is to provide more reliable nonlinear viscous drag forces compared to OpenFAST

3.2 Platform hydrostatics & hydrodynamics

Platform hydrostatics and hydrodynamics are solved by 3D panel program WAMIT. Fig. 5 shows

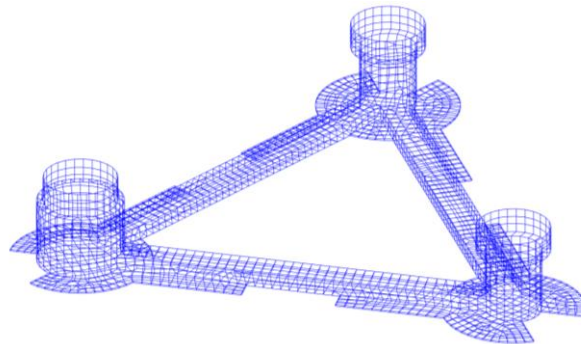


Fig. 5 CNOOC semisubmersible panel model (3674 constant panels) used for WAMIT

the panel geometry of the CNOOC semisubmersible platform. Total 3674 constant panels are used for the hydrostatics and hydrodynamics (diffraction and radiation) analysis. The estimated center of buoyancy is (43.32 m, 0 m, -11.54 m) from the origin. As described above, the coordinate origin is at MWL and center of the main column on which turbine is mounted. In this study, we employed the Newman's approximation for the 2nd-order difference-frequency wave force calculations instead of using full quadratic transfer function (QTF). It should be noted that we first performed the static-offset and free-decay tests to check the system's stiffness, damping, and natural period. The inertia (1 + added mass coefficient) and drag coefficients for each section of mooring line are given in Table 4.

3.3. Uncoupled and coupled free-decay tests: Viscous modeling of Morison members

The present hull form contains several heave-damping plates, whose drag coefficients are not well defined in the open literature. To estimate the drag coefficients of the Morison truss and heave-plate members, physical tank test was performed based on 1:64 scaled semisubmersible model. The semi-submersible platform model is designed and manufactured based on the design drawings provided by CNOOC (China) Co., Ltd. Beijing Research Center. The free-decay test was performed at Shanghai Jiao-tong University by CNOOC engineers only for the floating foundation without tower, RNA, and mooring lines. Instead, the tower and RNA weights were artificially added in the experiment to achieve the target hull draft, as shown in Fig. 6 since the objective of the experiment is focused on quantifying the heave-plate damping. The hull material in the tank test was made of carbon fiber and its motions were measured by an optical-tracking system. The wave tank size was 50 m in length and 40 m in width to ensure no reflection of motion induced waves from the walls during the time of free-decay test. The model was placed at its center region. Prior to the actual testing, the accuracy of the motion measurement was carefully checked.

The free-decay test was performed for heave, roll, and pitch DOFs. Based on the free-decay results, we estimated reasonable Morison drag coefficients of the truss and plate members. The same numerical free-decay was also done using the CHARM3D time-domain simulation. The results are summarized in Table 5(c). Next, the entire system with the hull, tower, RNA, and mooring lines are numerically modeled by CHARM3D-FAST as designed by CNOOC. For double-checking, the turbine-hull-mooring coupled free-decay simulations were also performed numerically by using another commercial program OrcaFlex after applying the same inputs.

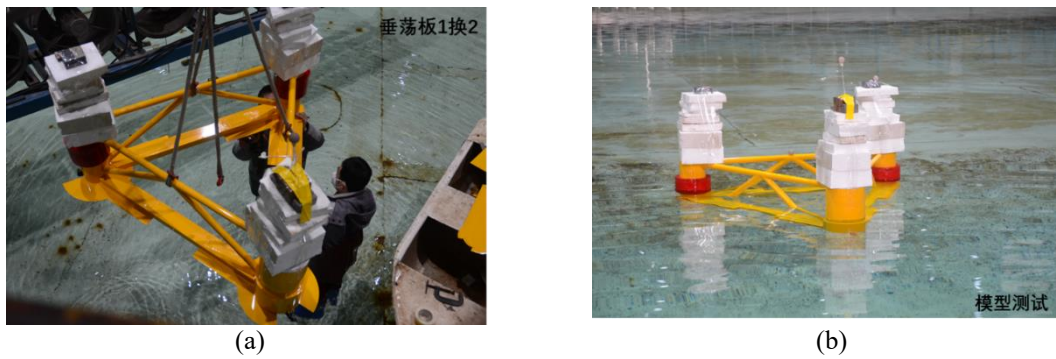


Fig. 6 Installation of the CNOOC 15MW Semi floating foundation (1:64 scale) into the 3D wave tank: (a) during installation (b) after installation

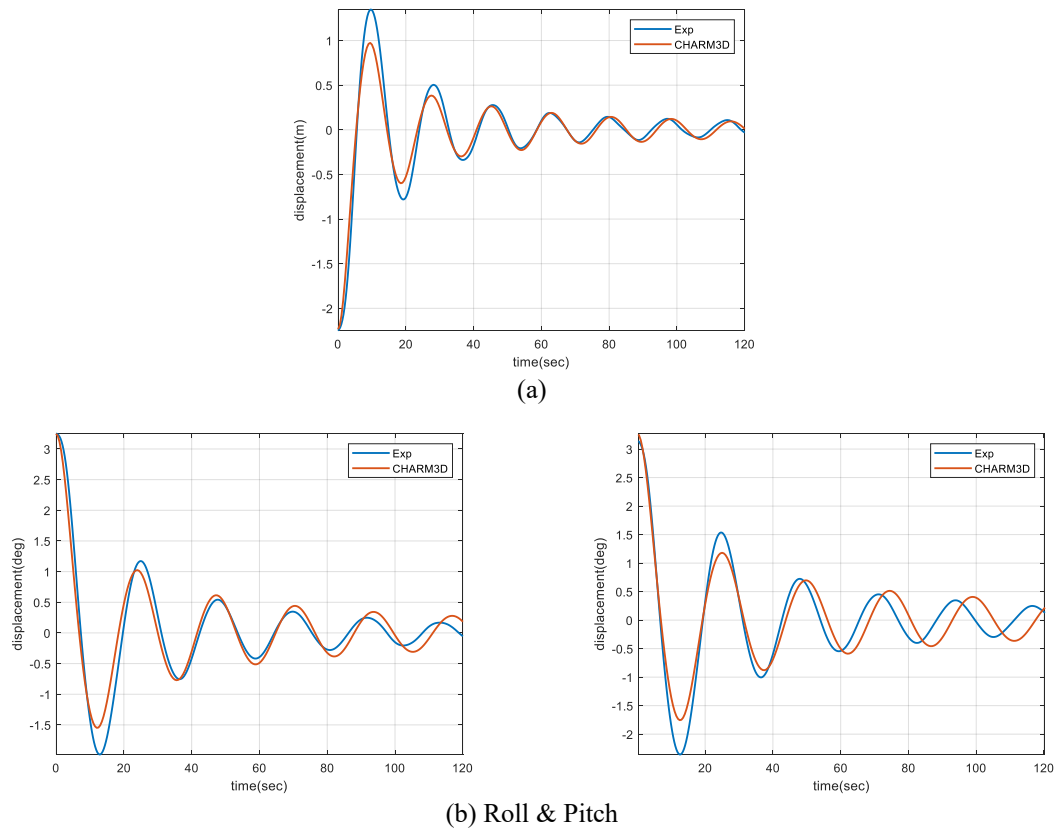


Fig. 7 Free-decay result: Experiment vs CHARM3D

3.3.1 Uncoupled (floating foundation only without mooring) free-decay test: Model test vs CHARM3D simulation

Fig. 2 shows the scaled semisubmersible physical-test hull model without and with heave plates. This model is slightly different from the panel geometry shown in Fig. 5 in that multiple slender braces are connected between the three columns. Those slender braces are not included in the panel-

related hydrodynamics calculations since their role is negligible in that regard. Table 5(a) and 5(b) shows the details about the scaled target and measured dimensions and relevant errors. Table 5c shows the estimated Morison drag coefficients for respective elements. The heave plate drag coefficient of 15 was estimated, which is consistent with the suggested range of drag coefficient determined through a series of experiment (Jang *et al.* 2019). The free-decay time-history results for the model test and Charm3D simulation are shown in Fig. 7, in which the numerical simulation is based on the estimated drag coefficients of Table 5(c). Due to the asymmetry of the hull form with respect to the y-axis, the heave and pitch DOFs are strongly coupled with each other. To avoid the pitch DOF's effect in heave free-decay test, the heave results were presented with respect to the pitch center of rotation ($x=6.51$ m, $y=0$ m, $z=11.2$ m). Fig. 7 and Table 6 show that the comparisons between the physical and numerical free-decay results are reasonably well matched.

Table 5 (a) Prototype vs Tank-test Model (1:64 scale)

Parameters	Target value		Measured	
	Prototype (m)	Model (m)	Measured (m)	Error (%)
Column spacing	86.00	1.344	1.343	-7.44E-4
Column 1 diameter	15.00	0.234	0.234	0
Column 1 lower part diameter	17.00	0.266	0.266	0
Column 2 diameter	11.00	0.172	0.172	0
Column 3 diameter	11.00	0.172	0.172	0
Column height	30.00	0.469	0.469	0
Column sleeve diameter	15.00	0.234	0.234	0
Sleeve height	10	0.156	0.155	-6.41E-3

Table 5 (b) Target values of the mass properties in the 1:64-scale physical experiment

Parameter	Unit	Prototype values	Target model values	Measured model values	Error	
Mass	kg	12521040	46.599	46.600	0.002%	
VCG	m	29.2 (From keel)	0.456	0.457	0.20%	
Radii of gyration	Rxx	m	35.0	0.547	0.553	1.22%
	Ryy	m	40.0	0.625	0.614	-1.78%
GM	m	33.93	0.530	0.522	-1.45%	

Table 5 (c) Drag coefficients for Morison plate members obtained from the free-decay test

Morison Type	Component	C_D
Truss members	Column 1	0.6
	Column 2, 3	0.6
	Pontoon	3.0
Plate members	Heave plate (Circular + rectangular)	15.0
	Footing (cylinder bottom)	3.0
	Disk-shaped discontinuous section b/w - upper & lower column (main)	3.0
	- sleeve & upper/lower columns (side)	

Table 6 Free-decay result: Experiment vs CHARM3D (floating foundation only)

	Natural Period (s) (Relative error)			Damping ratio (%)	
	Target	Model test	CHARM3D	Model test	CHARM3D
Heave	18.84	17.73 (5.89 %)	17.9 (4.99%)	9.42	8.89
Roll	22.1	22.66 (2.53%)	23.5 (6.33%)	9.39	7.80
Pitch	23.0	23.30 (1.30%)	24.7 (7.39%)	8.05	7.31

Table 7 Coupled free-decay test (entire system including turbine, floating foundation, and mooring): Natural periods and damping ratios for 6-DOFs (averaged for first 5 cycles)

	Natural Period (seconds)		Damping ratio (%)	
	OrcaFlex	CHARM3D-FAST	OrcaFlex	CHARM3D-FAST
Surge	60.8 (0.10 rad/s)	59.6	9.31	9.37
Sway	59.6	60.3	9.93	9.61
Heave	19.1 (0.33 rad/s)	19.1	9.78	9.81
Roll	28.2	27.8	9.97	9.24
Pitch	30.0 (0.21 rad/s)	30.7	8.86	9.21
Yaw (4-cycle avg.)	98.9	99.9	8.16	7.69

3.3.2 Coupled numerical free-decay tests for the entire system: Charm3D-FAST and OrcaFlex

Next, the numerical free-decay test was conducted for the entire system including floating foundation, mooring, tower, and RNA. The design parameters of the entire system is given in Table 1. For double checking, the coupled free-decay tests were performed numerically based on two independent computer simulation programs, Charm3D-FAST and OrcaFlex. The center of gravity is at the same horizontal location of the center of buoyancy ($x=43.325$ m, $y=0$ m, $z=11.2$ m) so that the even keel condition can be ensured in calm water. The mooring line consists of chain (top), steel wire (middle), and chain (seabed). Near the touchdown point, heavy clump weight on the bottom chain was used, for which both CHARM3D-FAST and OrcaFlex used quadratic-order spring. Also, we have checked the natural periods of all DOFs. Fig. 8 shows the coupled free-decay results for 6-DOFs and the corresponding natural periods and damping ratios averaged over first 5 peaks. The damping ratio was estimated based on the method of logarithmic decrement. The two independent simulation programs produced similar results. The values are summarized in Table 7.

3.3.3 Static Offset Test for the entire system by CHARM3D-FAST

To find out the system stiffness of the platform with mooring lines, static-offset tests were conducted numerically by using CHARM3D-FAST as shown in Fig. 9. The determined equivalent linear stiffness of the mooring system was inputted in the frequency-domain WAMIT calculation as external stiffness. Surge mooring stiffness shows the hardening behavior, which is the typical of chain catenary mooring in shallow water. Other modes exhibit linear-like behaviors. In the next section, it will be shown that the frequency-domain WAMIT results agree well with time-domain-

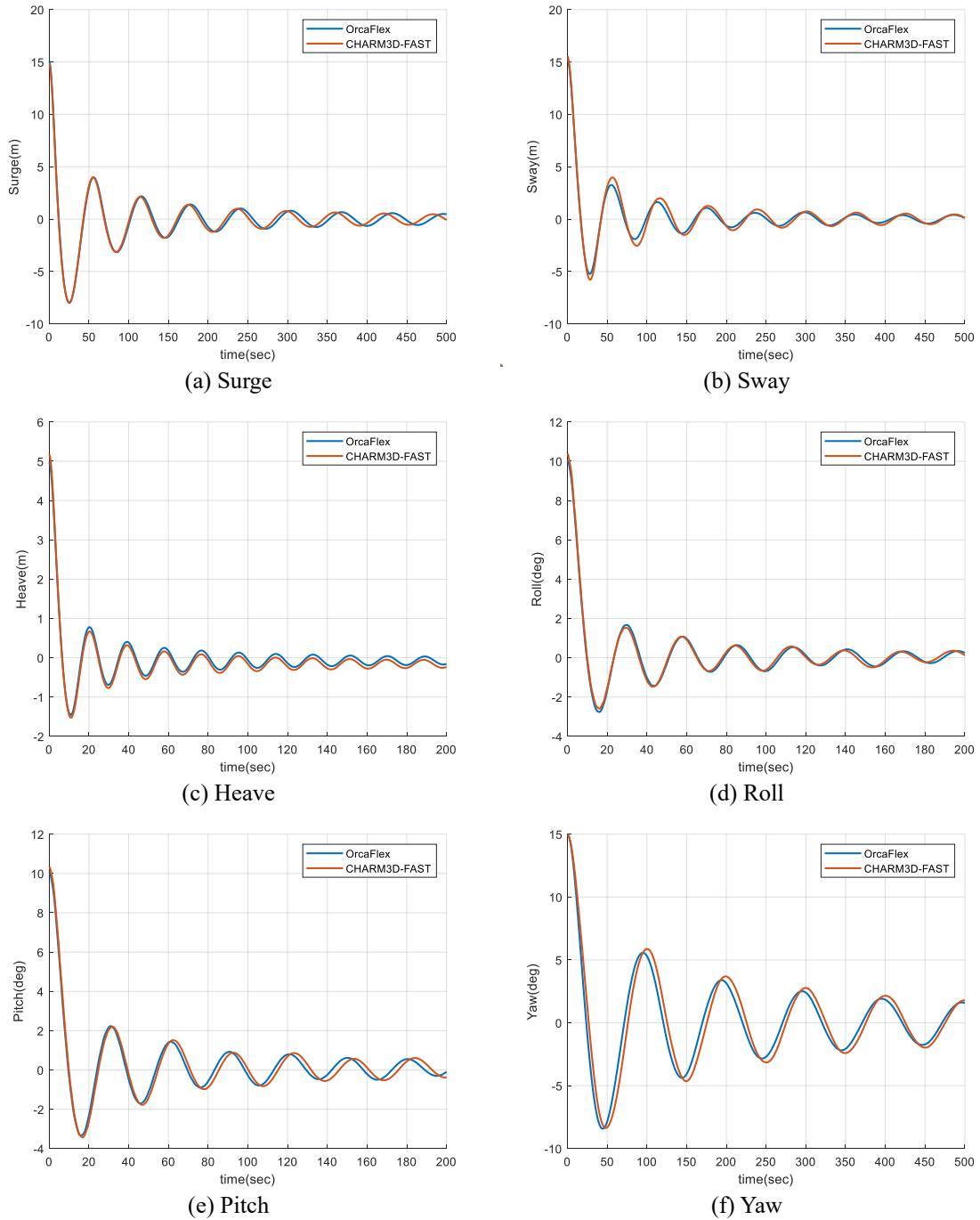


Fig. 8 Free-decay tests

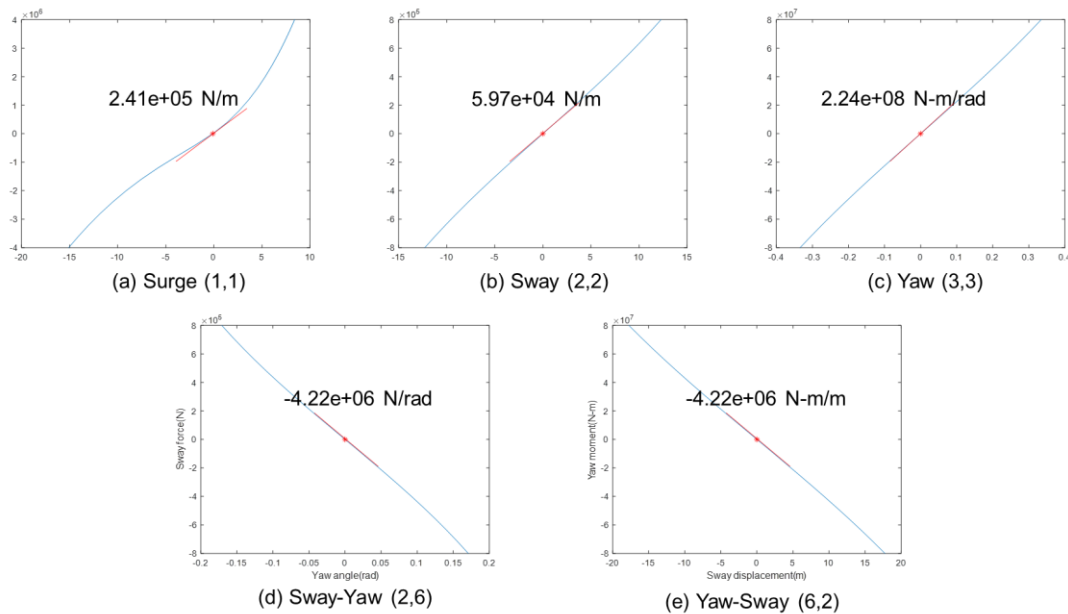


Fig. 9 Static-offset-test results of surge, sway, yaw and their coupling terms

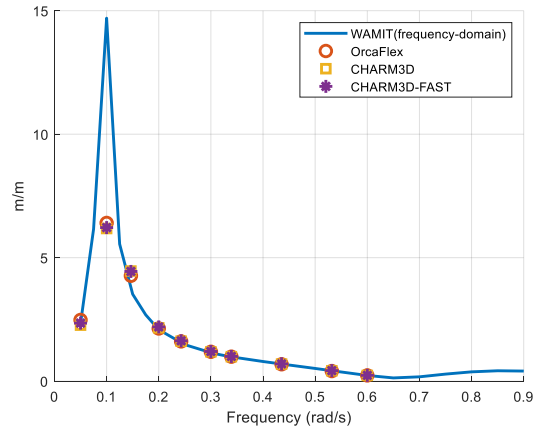
simulation results with mooring when all 6x6 mooring-stiffness modes are included. This is mainly due to the effect of heavy clump near mooring touch-down point, which makes the mooring system like taut mooring instead of slack catenary mooring and thereby mooring stiffness matrix components for non-planar DOFs (heave, roll, pitch) are non-negligible.

4. Numerical simulations and results

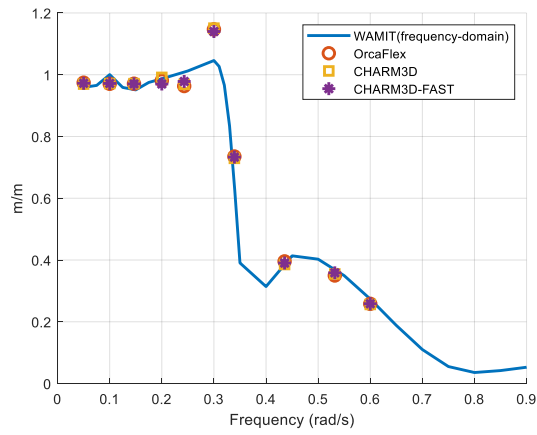
4.1 Regular wave case

From this point on, all the numerical results are for the entire system including floating foundation, mooring, tower, and RNA. To validate the developed numerical FOWT model in the FAST-CHARM3D, we compared the results with another independent commercial program OrcaFlex. In the above simulation programs, the elastic behaviors of tower and blades are included. To demonstrate the tower/blade elasticity effects, another simulation called CHARM3D was also conducted assuming that the entire system is a rigid body with 6 rigid modes.

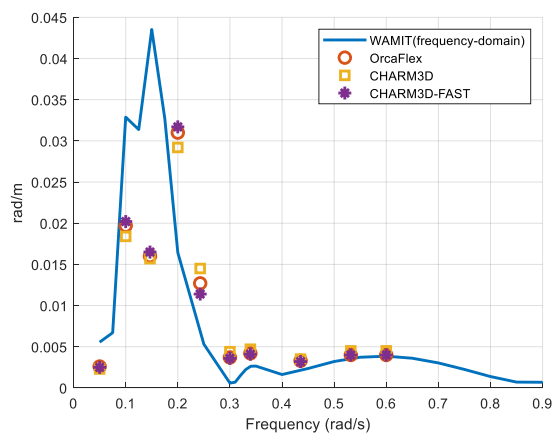
We first performed regular-wave simulations for several wave periods. Also, the frequency-domain RAOs are generated with 6x6 mooring stiffness matrix obtained by OrcaFlex as input to the frequency-domain diffraction/radiation program WAMIT and it is compared with the corresponding time-domain simulation results. It is normal to consider only the mooring stiffness of the planar motions (surge, sway and yaw) for catenary-type mooring system based on the static offset test, so we first inputted surge, sway and yaw stiffness to the frequency-domain panel program WAMIT. However, it has been found that the present mooring system's heavy clumps at bottom chain can largely affect the coupled system stiffness for not only surge/sway/roll but also non-planar DOFs



(a) Surge RAO



(b) Heave RAO at (53 m, 0 m, 0 m)



(c) Pitch RAO

Fig. 10 FOWT RAOs in 0 deg. wave heading

(heave, roll, and pitch) like a taut or semi-taut mooring system. Indeed, the frequency-domain RAOs with 6x6 external mooring stiffness matrix generally match better against time-domain simulation results especially in the low-frequency region. The frequency-domain RAOs are generated by running WAMIT to calculate hydrodynamic coefficients and diffraction loads with respect to the center of rotation, say, $x=53$ m from the main column. This is because the diagonal part of the free-decay damping coefficient (e.g., Table 7) can be employed in a consistent manner. Otherwise, off-diagonal elements of the external damping matrix could be needed.

Fig. 10 shows RAOs for surge, heave, and pitch DOFs. In Fig. 10(a), the overall trends for surge results agree well among the programs. The linear-potential-flow result WAMIT overpredicts the peak amplitude compared to other time-domain simulations including nonlinear drags. In Fig. 10(b), again, WAMIT results agree well with time-domain results except the difference at the peak. Fig. 10(c) presents the pitch RAO where all the time-domain results are generally well-matched with each other showing two peaks at surge (0.1 rad/s) and pitch (0.2 rad/s) natural frequencies. However, in the frequency-domain WAMIT pitch RAO, this feature is less pronounced. In the pitch RAO case, we see nontrivial differences between CHARM3D-FAST (tower-flexible) and CHARM3D (tower-rigid) near the peaks, which can be attributed to the tower-elasticity effects.

4.2 Irregular wave test: Survival condition (50-year return period)

An irregular wave test was performed for the survival loading case of 50 years of return period (YRP). We assumed that the corresponding wind/wave/current are collinear and incident from head direction (0 deg.). The detailed simulation condition is given in Table 8 below. The turbulence full-field wind input files are generated using TurbSim for 5 random seeds. Although the EWM (Extreme Wind Model) is valid only for 10 minutes, we increased the simulation time up to 1 hour. The turbine is in an idling condition which is suitable for extreme environments instead of standstill locked condition. JONSWAP wave spectrum of $H_s=11.5$ m and $T_p=14.2$ sec. ($=0.44$ rad/s) is used with peak enhancement parameter of 2.4. Wave cut-off frequency is 0.15 rad/s to 1.4 rad/s and 61 component waves are generated in CHARM3D-FAST with randomly perturbed frequency interval to avoid signal repetition. In the OrcaFlex run, 100 component waves were used with equal energy discretization. Total 5 sets of random-phase seeds were generated for both CHARM3D-FAST and OrcaFlex runs. The generated wave time series and reconstructed wave amplitude spectrum are shown in Fig. 10(a) and 10(b).

For the simulation of dynamic wind, full-field binary type undisturbed wind inflow files (extension “.bts”) were generated by NREL-developed program “TurbSim”, which is compatible with AeroDyn module as a sub-part of FAST. The IEC Kaimal model is used for the turbulence flow spectrum (Jonkman 2009):

$$S(f) = \frac{4\sigma^2 (L/V_{hub})}{[1 + 6f \cdot (L/V_{hub})]^{5/3}} \quad \text{with} \quad \sigma = \frac{TI}{100} V_{hub}$$

where f is cyclic frequency, L is an integral scale parameter dependent on the hub-height, and u_{hub} is mean wind-speed at the hub-height. σ is standard deviation relevant to the turbulence intensity $TI(\%)$. The input theoretical and regenerated wind spectra are shown in Fig. 10(c). Winds produce excitations at much lower frequencies than waves.

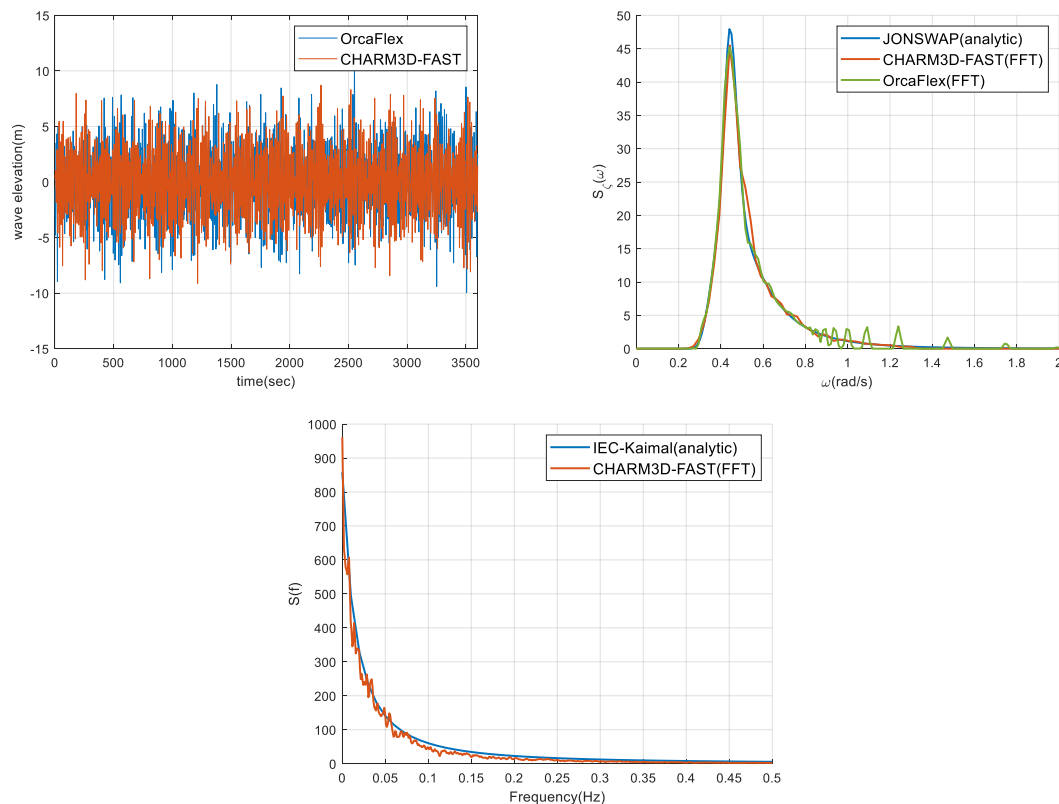
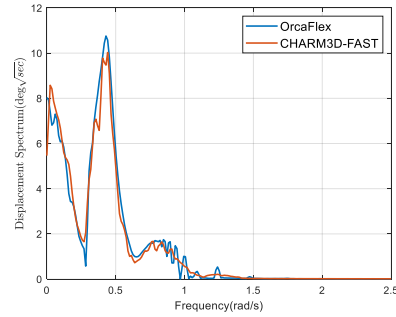
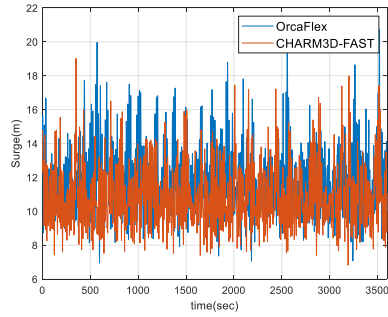


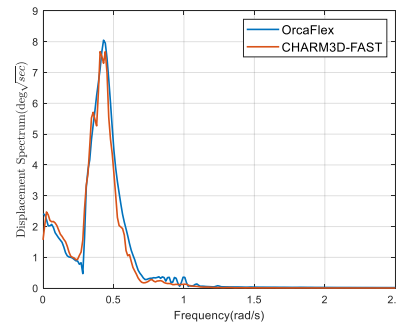
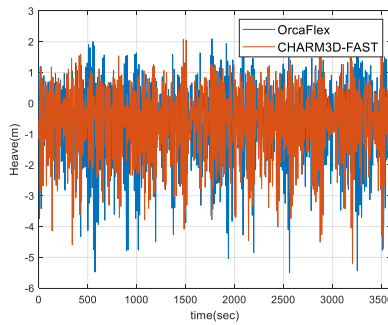
Fig. 11 Wave elevation at origin (0,0,0) of global coordinate system: Time-series (top left) and JONSWAP and regenerated wave amplitude spectra (top right) by CHARM3D-FAST and OrcaFlex; realized with 1 seed for time-series and 5 seeds for spectrum. Theoretical and regenerated wind spectra (bottom)

Fig. 11 shows the time-series and spectra for 4-DOF (surge, heave, pitch and yaw) motions in the applied survival condition. Due to the geometric symmetry, sway and roll motions are to be small. In overall, the two independent simulation results show good agreements. The surge mean displacement is slightly larger in the case of OrcaFlex. In Fig. 11(b), the CHARM3D-FAST and OrcaFlex heave responses are almost similar. In Fig. 11(c), the OrcaFlex shows a little larger low-frequency pitch response. Both programs show that the maximum (absolute) pitch values are less than 10 degrees, which is acceptable considering the pitch design criteria. Fig. 11(d) shows the yaw time-series and corresponding spectra. Since the full-field wind considers lateral turbulence fluctuations with 8.6% turbulence intensity, yaw motion can be generated even for 0-degree heading.

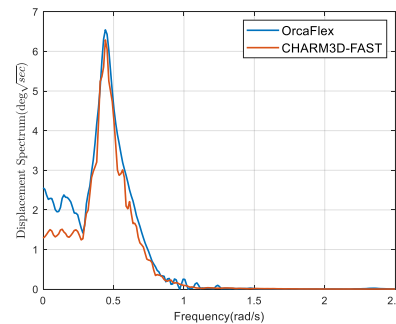
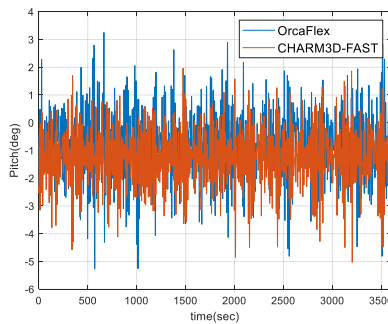
The yaw-motion spectra resemble the input wind spectra since yaw motion is mostly triggered by wind. The maximum yaw value is 4.7 degrees in CHARM3D-FAST but 3.4 degrees in OrcaFlex. Also, in Table 10, the statistical values of horizontal offsets are given. The maximum offset in OrcaFlex is 21.4 m while that in CHARM3D-FAST is 19.6 m. This difference might be caused by different numerical modeling for mooring lines and clumps. The CHARM3D-FAST employs higher-order rod FE whereas the OrcaFlex uses lumped-mass-spring approach. Indeed, we noticed the difference in surge free-decay result in Table 7 where CHARM3D-FAST has slightly smaller natural period meaning that the mooring lines are a bit stiffer than that of the OrcaFlex.



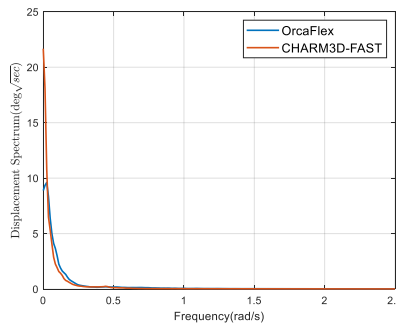
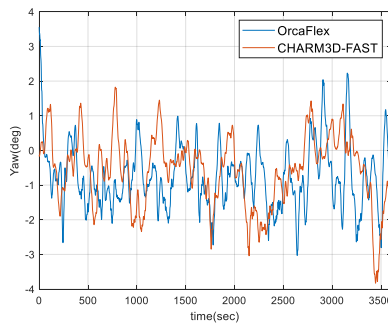
(a) Surge



(b) Heave at (53 m, 0 m, 0 m)



(c) Pitch



(d) Yaw

Fig. 12 Motion responses (50-yr storm): Time-series (left) and Displacement spectrum (right) (realized with 1 seed for time-series and 5 seeds for spectrum)

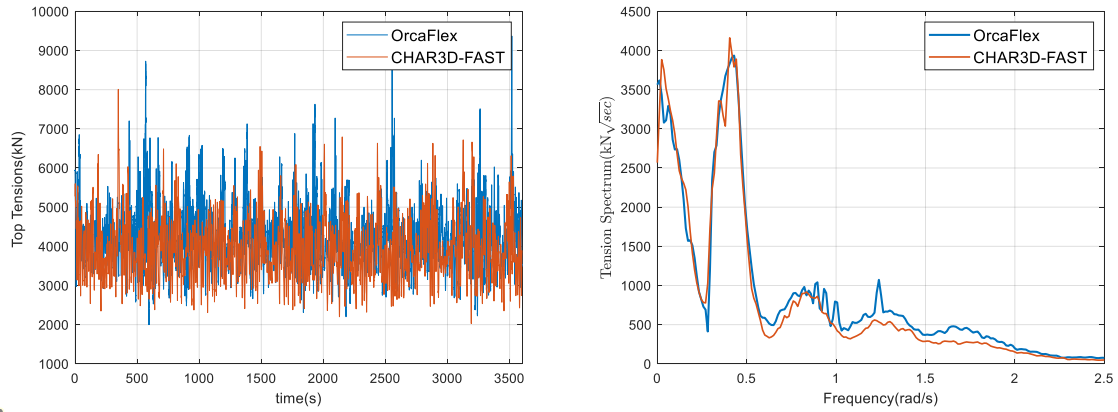


Fig. 13 Taut-side mooring top-tension LEG#1: Time-series (left) and Tension spectrum (right) (realized with 1 seed for time-series and 5 seeds for spectrum)

Table 8 Simulation case: survival condition (50-yr storm)

Simulation time	Wind (EWM)	Wave (ESS)	Current	Turbine condition	Description	Weather direction (deg.)
3600s	52.1 m/s (11% TI)	Hs = 11.5 m, Tp = 14.2s	2.1 m/s (1/7 exp. law)	Idling	50YRP	0

*EWM: Extreme Wind Model; ESS: Extreme Sea-State; TI: Turbulence Intensity

Table 9 Motion statistics (averaged over 5 random seeds)

DOFs	Value	OrcaFlex	CHARM3D-FAST
Surge (m)	STD	1.93	1.85
	MEAN	11.79	10.97
	MAX	21.37	19.52
	MIN	7.10	6.90
Heave (m)	STD	1.22	1.15
	MEAN	-0.76	-0.76
	MAX	2.23	2.22
	MIN	-6.09	-5.78
Pitch (deg.)	STD	1.10	0.95
	MEAN	-0.83	-1.27
	MAX	3.67	2.30
	MIN	-5.41	-5.41
Yaw (deg.)	STD	0.90	1.23
	MEAN	-0.79	-0.55
	MAX	2.59	2.60
	MIN	-3.43	-4.74

Table 10 Horizontal offset statistics

	Value	OrcaFlex	CHARM3D-FAST
Offset (m)	STD	1.92	1.85
	MEAN	11.84	11.07
	MAX	21.40	19.62

Table 11 Mooring top-tension statistics (averaged over 5 random seeds)

LEG #	Value	OrcaFlex	CHARM3D-FAST
LEG1 (kN)	STD	8.29E+02	8.13E+02
	MEAN	4.28E+03	3.93E+03
	MAX	1.03E+04	8.52E+03

* MBL: 1.83E+4 kN (R3S Chain) / Allowable tension (safety factor 1.67): 1.10E+04 kN

 Table 12 Tower/Blade Properties and natural frequencies (Allen *et al.* 2020, Gaertner *et al.* 2020)

Classification	Parameter	Units	Value
Tower	Mass	t	1263
	Length from tower base to tower top	m	129.495
	1st fore-aft bending mode natural frequency	rad/s	3.12
	1st side-side bending mode natural frequency	rad/s	3.03
	Blade	Mass (for each blade)	t
Blade	Length from blade root to blade edge	m	117
	1st flap-wise mode natural frequency	rad/s	3.49
	1st edgewise mode natural frequency	rad/s	4.03

Lastly, the mooring top-tension is shown in Fig. 12 and their statistical values are given in Table 11. It is observed that the taut-side mooring #1 is the most critical out of the 6 legs. Due to the larger offset by OrcaFlex, it gives higher maximum mooring tension than CHARM3D-FAST, i.e., 10.3 MN (OrcaFlex) vs. 8.5 MN (CHARM3D-FAST), both of which are less than the current-mooring allowable tension (breaking strength divided by safety factor 1.67) of 11.0MN. This means that the current mooring design satisfies the applied 50-yr storm condition.

4.3 Comparison between flexible and rigid tower

Next, let us consider the comparison between turbine-mooring-floating foundation full-coupled dynamic analysis including tower-blade elasticity and a simpler approximation method to treat the whole turbine as a rigid body, for which tower elasticity is not included.

To avoid dynamic resonance between tower and blades, the tower was conservatively designed

Table 13 Steel Material Properties for the Tower (Allen *et al.* 2020)

Parameter	Units	Value
Young's Modulus	Pa	200E+11
Shear Modulus	Pa	793E+10
Density	kg/m ³	785E+03

Table 14 Rigid vs Flexible: statistics (Survival condition 50-yr storm)

Parameter	Value	Units	Rigid	Flexible
Platform pitch angular displacement, θ	STD	degree	0.97	0.95
	MEAN		-1.20	-1.27
	MAX		2.45	2.30
	MIN		-5.39	-5.41
Tower fore-aft bending moment, My	STD	kN-m	1.13E+05	1.19E+05
	MEAN		-7.90E+04	-8.38E+04
	MAX		3.76E+05	4.18E+05
	MIN		-5.41E+05	-6.18E+05
x-direction acceleration at yaw-bearing (tower-top), A_x	STD	m/sec ²	0.51	0.55
	MEAN		0.0	0.01
	MAX		1.99	2.48
	MIN		-2.13	-2.47
y-direction acceleration at yaw-bearing (tower-top), A_y	STD	m/sec ²	0.08	0.21
	MEAN		0.0	0.0
	MAX		0.34	0.95
	MIN		-0.47	-0.94

to have the 1st fore-aft and side-side natural frequencies (around 0.5 Hz) higher than rotational speeds of one blade (1P) ranging (0.06~0.14 Hz) and 3 blades (3P) ranging (0.2~0.4 Hz), taking the increased rotor speed variability into account. (Allen *et al.* 2020). The same strategy was also used in the present design.

The tower base height is 15 m and the hub height is 150 m above MWL. The total flexible tower length is 129.49 m from the tower base to tower top (yaw-bearing). The tower and blade lowest natural frequencies and their materials are summarized in Tables 12 and 13.

Fig.13 shows the comparisons of tower-base bending moments and nacelle accelerations between the fully-coupled and tower-rigid-body approach. It is seen that the platform pitch motions are about the same, which means that tower flexibility does not influence the floater motions. On the other hand, the tower-base bending moments and nacelle accelerations are appreciably affected by tower flexibility. In particular, the appearance of a clear peak near the lowest tower bending mode (around 3 rad/s) is noticeable both in the bending moment and nacelle acceleration. Despite that the incident wave spectrum was truncated at 1.6 rad/s in the simulation, we still observe tower/blade resonances at much higher frequencies, which might be induced by nonlinear Morison wave forces and wind

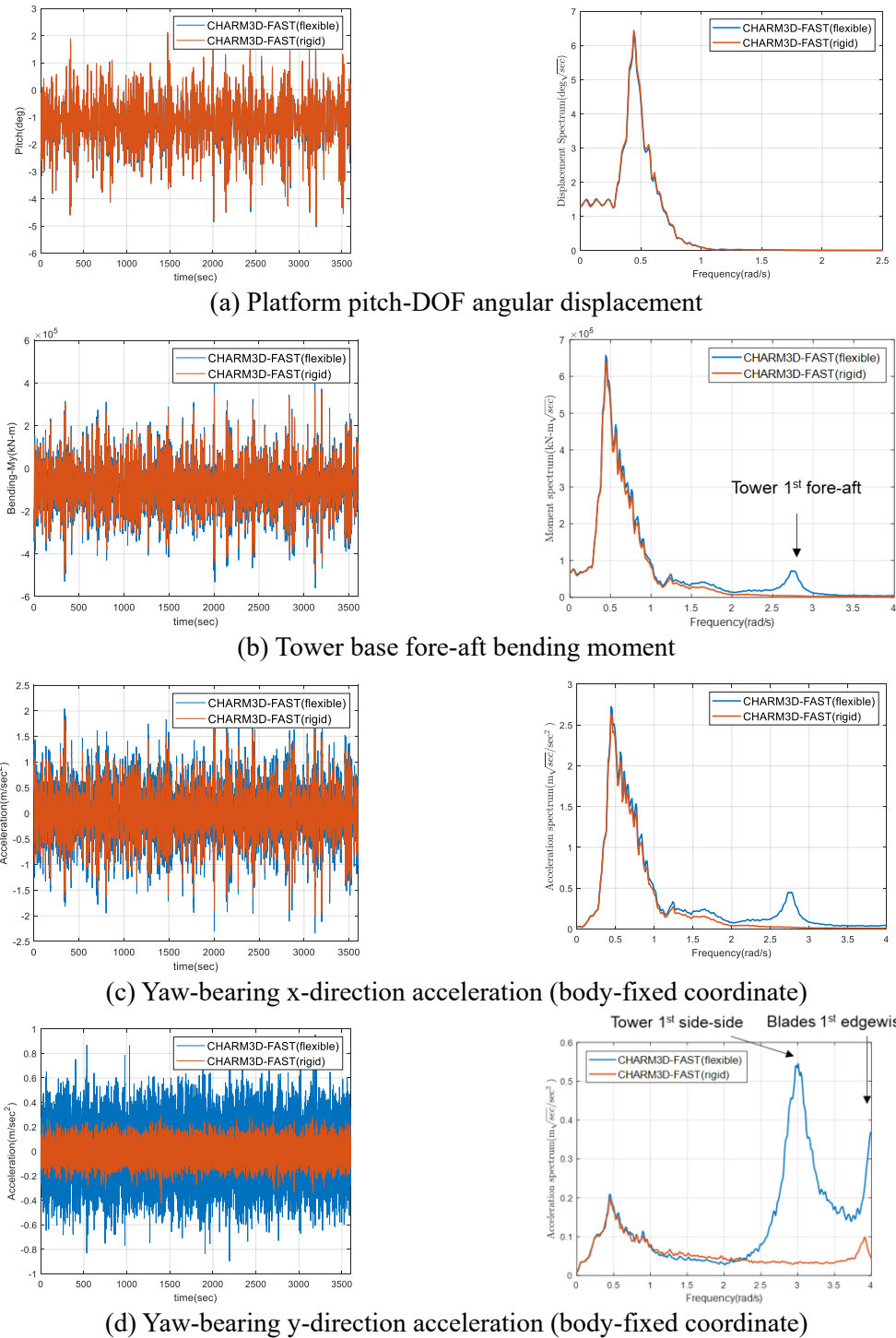
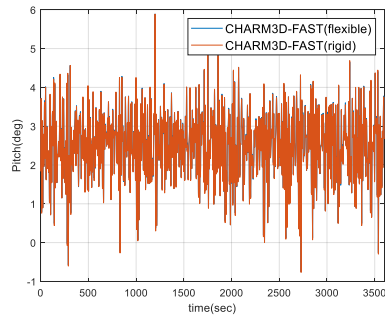
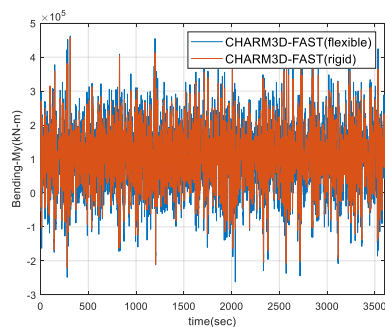
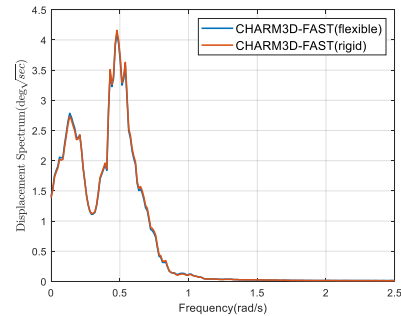


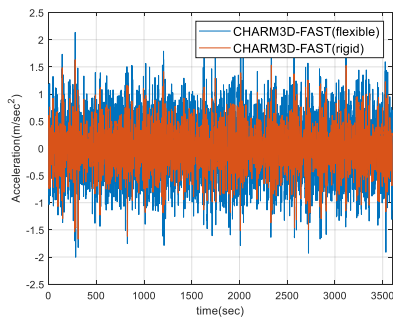
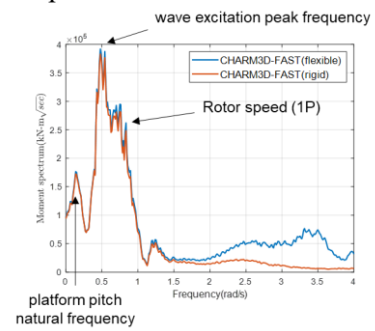
Fig. 14 Time-series (left) and moment spectrum (right) for 50-yr storm; realized with 1 seed for time-series and 5 seeds for spectrum



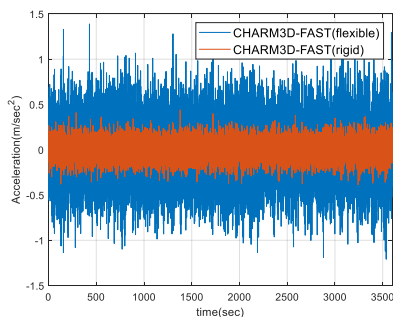
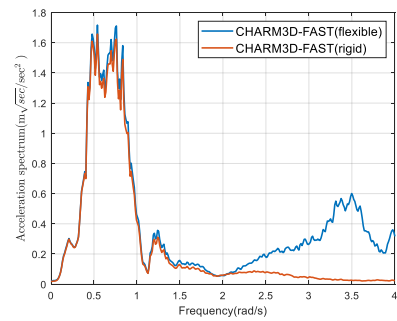
(a) Platform pitch-DOF angular displacement



(b) Tower base fore-aft bending moment



(c) Yaw-bearing x-direction acceleration (body-fixed coordinate)



(d) Yaw-bearing y-direction acceleration (body-fixed coordinate)

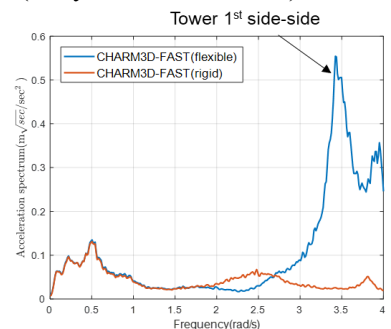


Fig. 15 Time-series (left) and moment spectrum (right) for maximum operational condition; realized with 1 seed for time-series and 5 seeds for spectrum

Table 15 Maximum operating condition (DLC1.6): CHARM3D-FAST

Relevant DLC #	Duration (sec)	Wind	Wave	Current (m/s)	Turbine condition	Description	Controller
1.6	3600	NTM (=25.0 m/s, 13% TI)	SSS (Hs = 9.0 m / Tp = 12.9s)	0.85	Operating	$V_{hub} = V_{cut-out}$	ROSCO (blade-pitch, variable-speed torque)

Table 16 Rigid vs Flexible: statistics summary DLC 1.6 (Maximum operating condition)

Parameter	Value	Units	Rigid	Flexible
Platform pitch angular displacement, θ	STD		0.80	0.79
	MEAN	degree	2.50	2.50
	MAX		5.31	5.29
	MIN		-1.02	-0.99
Tower fore-aft bending moment, My	STD			8.64E+04
	MEAN	kN-m	1.06E+05	1.07E+05
	MAX		4.59E+05	4.94E+05
	MIN		-2.40E+05	-2.83E+05
x-direction acceleration at yaw-bearing (tower-top), A_x	STD			0.41
	MEAN	m/sec ²	0.00	0.0
	MAX		1.63	2.11
	MIN		-1.69	-2.03
y-direction acceleration at yaw-bearing (tower-top), A_y	STD			0.10
	MEAN	m/sec ²	0.00	0.0
	MAX		0.45	1.31
	MIN		-0.41	-1.36

turbulence excitations. The increase of nacelle (yaw-bearing) acceleration causes the increase of the corresponding inertia force, which can affect the fatigue life of tower. The corresponding statistics are summarized in Table 14. The maximum x- and y-directional nacelle accelerations are increased by 16% and 102% in case of flexible tower compared to the rigid-tower case.

Next, let us consider the same comparison in the case of maximum operation condition, which are presented in Fig. 14. The corresponding environmental conditions are summarized in Table 15. Since we assumed mean wind speed as cut-out speed at hub-height, blade-pitch controller is considered to maintain averaged 15-MW power output. The overall trends are similar to those of Fig. 13. There are several differences in this case though compared to the survival condition. In this case, the blades are not in idle condition but rotating with blade-pitch-angle control to generate the rated power. Due to relatively larger wind loading on the blades, there exist increased influences of 1P and 3P effects on tower-base bending moment and nacelle acceleration in a wide range of high frequencies. 1P effect shows noticeable peak near wave peak frequency while 3P effect is distributed over high frequencies between 1P and the lowest tower natural frequency. The corresponding

statistics are summarized in Table 16. The maximum x- and y-directional nacelle accelerations are increased by 25% and 202% in case of flexible tower compared to rigid tower.

5. Conclusions

In this study, a 15MW semisubmersible FOWT in 100m water depth was investigated. Through in-house turbine-floater-mooring fully-coupled dynamics simulation program, the feasibility and global performance of the FOWT under combined extreme wind/wave/current condition was analyzed. For double-checking, the same cases were also run by a commercial program OrcaFlex and their results were mutually validated and systematically compared. The unique feature of the FOWT is the use of many heave damping plates on its hull and their proper viscous drag coefficients were obtained through comparison with free-decay test in a 3D wave basin using 1:64-scaled physical model. Through this study, we have observed the following:

1. The two independent computer simulation programs, CHARM3D-FAST and OrcaFlex, produced consistent results compared to each other and against physical experimental results.

2. The noticeable differences between the two programs can be seen in maximum surge offsets and the corresponding mean mooring tensions. This caused 20% higher mooring top-tension in OrcaFlex compared to CHARM3D-FAST for the survival condition.

3. The effect of tower flexibility was investigated by comparing tower-base fore-aft bending moment and nacelle translational accelerations. The tower flexibility little influence floater motions in semi-submersible FOWT. Due to the tower flexibility, the maximum x- and y-directional nacelle accelerations are increased by 16% and 102% in survival condition and 25% and 202% in maximal operational condition. The increase of nacelle accelerations causes the increase of the corresponding inertia force, which can affect the fatigue life of tower.

References

- Abbas, N.J., Zalkind, D.S., Pao, L. and Wright, A. (2022), "A reference open-source controller for fixed and floating offshore wind turbines", *Wind Energy Sci.*, **7**(1), 53-73. <https://doi.org/10.5194/wes-7-53-2022>.
- Abdelmoteleb, S.E., Mendoza, A.S.E., dos Santos, C.R., Bachynski-Polić, E.E., Griffith, D.T. and Oggiano, L. (2022), "Preliminary sizing and optimization of semisubmersible substructures for future generation offshore wind turbines", *J. Physics: Conference Series*.
- Allen, C., Viscelli, A., Dagher, H., Goupee, A., Gaertner, E., Abbas, N., Hall, M. and Barter, G. (2020), Definition of the UMaine VoltturnUS-S reference platform developed for the IEA wind 15-megawatt offshore reference wind turbine, National Renewable Energy Lab.(NREL), Golden, CO (United States); Univ. of Maine.
- Arcandra and Kim, M.H. (2003), "Hull/mooring/riser coupled dynamic analysis and sensitivity study of a tankerbased FPSO", *Appl. Ocean Res.*, **25**, 367-382. <https://doi.org/10.1016/j.apor.2003.02.001>.
- Bae, Y.H. and Kim, M.H. (2011), "Rotor-floater-mooring coupled dynamic analysis of mono-column-TLP-type FOWT (Floating Offshore Wind Turbine)", *Ocean Syst. Eng.*, **1**(1), 93-109. <https://doi.org/10.12989/ose.2011.1.1.093>.
- Bae, Y.H. and Kim, M.H. (2014), "Coupled dynamic analysis of multiple wind turbines on a large single floater", *Ocean Eng.*, **92**, 175-187.
- Bae, Y.H. and Kim, M.H. (2014), "Influence of control strategy to FOWT global performance by aero-elastic-control-floater-mooring coupled dynamic analysis", *J. Ocean Wind Energy*, **1**(1), 50-58
- Bae, Y.H., Kim, M.H. and Kim, H.C. (2017), "Performance changes of a floating offshore wind turbine with

- broken mooring line”, *Renew. Energ.*, **101**, 364-375. <https://doi.org/10.1016/j.renene.2016.08.044>.
- Bak, C., Zahle, F., Bitsche, R., Kim, T., Yde, A., Henriksen, L.C., Hansen, M.H., Blasques, J.P.A.A., Gaunaa, M. and Natarajan, A. (2013), “The DTU 10-MW reference wind turbine”, Danish wind power research 2013.
- Chen, J., Jin, C. and Kim, M.H. (2023), “Systematic comparisons among OpenFAST, Charm3D-FAST simulations and DeepCWind model test for 5 MW OC4 semisubmersible offshore wind turbine”, *Ocean Syst. Eng.*, **13**(2), 173-193. <https://doi.org/10.12989/ose.2023.13.2.173>.
- Cummins, W. (1962), “The impulse response function and ship motions”.
- DNVGL-ST-0119. (2021), “Floating wind turbine structures”
- DNV-ST-0437. (2016), “Loads and site conditions for wind turbines”
- EDP renewable (2020), Windfloat atlantic project starts supplying clean energy in Portugal. URL. <https://www.edpr.com/en/news/2020/01/02/windfloat-atlantic-project-starts-supplying-clean-energy-portugal>.
- Gaertner, E., Rinker, J., Sethuraman, L., Zahle, F., Anderson, B., Barter, G.E., Abbas, N.J., Meng, F., Bortolotti, P. and Skrzypinski, W. (2020), IEA wind TCP task 37: definition of the IEA 15-megawatt offshore reference wind turbine, National Renewable Energy Lab.(NREL), Golden, CO (United States).
- Garrett, D.L. (1982), “Dynamic analysis of slender rods”.
- Gomes, J.G., Lin, Y., Jiang, J., Yan, N., Dai, S. and Yang, T. (2022), “Review of offshore wind projects status: new approach of floating turbines”, *Proceedings of the 2022 5th International Conference on Power and Energy Applications (ICPEA)*.
- Huang, W.H. and Yang, R.Y. (2021), “Water depth variation influence on the mooring line design for FOWT within shallow water region”, *J. Mar. Sci. Eng.*, **9**(4), 409. <https://doi.org/10.3390/jmse9040409>.
- Islam, M.T. (2016), Design, Numerical Modelling and Analysis of a Semi-submersible Floater Supporting the DTU 10MW Wind Turbine (Ph.D. thesis). Norwegian University of Science and Technology, Trondheim, Norway.
- Jang, H.K., Park, S., Kim, M.H., Kim, K.H. and Hong, K. (2019), “Effects of heave plates on the global performance of a multi-unit floating offshore wind turbine”, *Renew. Energ.*, **134**, 526-537. <https://doi.org/10.1016/j.renene.2018.11.033>.
- Jonkman, B.J. (2009), TurbSim user's guide: Version 1.50, National Renewable Energy Lab.(NREL), Golden, CO (United States).
- Jonkman, J.M. and Buhl, M.L. (2005), FAST user's guide, National Renewable Energy Laboratory Golden, CO, USA.
- Jonkman, J.M., Butterfield, S., Musial, W. and Scott, G. (2009), Definition of a 5-MW reference wind turbine for offshore system development, National Renewable Energy Lab.(NREL), Golden, CO (United States).
- Jonkman, J.M. and Matha, D. (2011), “Dynamics of offshore floating wind turbines—analysis of three concepts”, *Wind Energy*, **14**(4), 557-569. <https://doi.org/10.1002/we.442>.
- Kikuchi, Y. and Ishihara, T. (2019), “Upscaling and leveled cost of energy for offshore wind turbines supported by semi-submersible floating platforms”, *J. Physics: Conference series*.
- Kim, H.C. and Kim, M.H. (2015), “Global performances of a semi-submersible 5 MW wind-turbine including second-order wave-diffraction effects”, *Ocean Syst. Eng.*, **5**(3), 139-160. <https://doi.org/10.12989/ose.2015.5.3.139>.
- Kim, H.C. and Kim, M.H. (2016), “Comparison of simulated platform dynamics in steady / dynamic winds and irregular waves for OC4 semi-submersible 5 MW wind-turbine against DeepCwind model-test results”, *Ocean Syst. Eng.*, **6**(1), 1-21. <https://doi.org/10.12989/ose.2016.6.1.001>.
- Kim, H.C., Kim, K.H., Kim, M.H. and Hong, K. (2017), “Global performance of a KRISO semisubmersible multiunit floating offshore wind turbine: Numerical simulation vs. model test”, *Int. J. Offshore Polar Eng.*, **27**(1), 70-81. <https://doi.org/10.17736/ijope.2017.fvr02>.
- Lee, I.J. and Kim, M.H. (2022), “Feasibility study for wrap-buoy assisted wet-tow and stepwise installation of mono-bucket foundation for 15MW offshore wind turbine”, *Ocean Syst. Eng.*, **12**(4), 413-437. <https://doi.org/10.12989/ose.2022.12.4.413>.
- Lopez-Pavon, C. and Souto-Iglesias, A. (2015), “Hydrodynamic coefficients and pressure loads on heave plates for semi-submersible floating offshore wind turbines: A comparative analysis using large scale

- models”, *Renew Energ*, **81**, 864-881. <https://doi.org/10.1016/j.renene.2015.04.003>.
- Mahfouz, M.Y., Molins, C., Trubat, P., Hernández, S., Vigara, F., Pegalajar-Jurado, A., Bredmose, H. and Salari, M. (2021), “Response of the International Energy Agency (IEA) Wind 15 MW WindCrete and Activefloat floating wind turbines to wind and second-order waves”, *Wind Energy Sci.*, **6**(3), 867-883.
- Moriarty, P.J. and Hansen, A.C. (2005), AeroDyn theory manual, National Renewable Energy Lab., Golden, CO (US)
- NREL (2023), OpenFAST. NREL, URL: <https://github.com/OpenFAST/openfast>.
- Orcina (2023), OrcaFlex, Orcina, <https://www.orcina.com/>
- Robertson, A., Jonkman, J., Masciola, M., Song, H., Goupee, A., Coulling, A. and Luan, C. (2014a), Definition of the semisubmersible floating system for phase II of OC4, National Renewable Energy Lab.(NREL), Golden, CO (United States)
- Robertson, A., Jonkman, J., Vorpahl, F., Popko, W., Qvist, J., Frøyd, L., Chen, X., Azcona, J., Uzunoglu, E. and Guedes Soares, C. (2014b), “Offshore code comparison collaboration continuation within IEA wind task 30: Phase II results regarding a floating semisubmersible wind system”, *Proceedings of the International Conference on Offshore Mechanics and Arctic Engineering*.
- Rinker, J., Gaertner, E., Zahle, F., Skrzypiński, W., Abbas, N., Bredmose, H., Barter, G. and Dykes, K. (2020), “Comparison of loads from HAWC2 and OpenFAST for the IEA Wind 15 MW Reference Wind Turbine”, J. Physics: Conference Series.
- Ran, Z. (2000), Coupled dynamic analysis of floating structures in waves and currents, Texas A&M University
- Shim, S. and Kim, M. (2008), “Rotor-floater-tether coupled dynamic analysis of offshore floating wind turbines”, *Proceedings of the ISOPE International Ocean and Polar Engineering Conference*.
- Tian, X. (2016), Design, Numerical Modelling and Analysis of TLP Floater Supporting the DTU 10MW Wind Turbine (Ph.D. thesis). Norwegian University of Science and Technology, Trondheim, Norway.
- Wang, L., Robertson, A., Jonkman, J. and Yu, Y.H. (2022), “OC6 phase I: Improvements to the OpenFAST predictions of nonlinear, low-frequency responses of a floating offshore wind turbine platform”, *Renew Energ.*, **187**, 282-301. <https://doi.org/10.1016/j.renene.2022.01.053>.
- Wu, J. and Kim, M.H. (2021), “Generic upscaling methodology of a floating offshore wind turbine”, *Energies*, **14**(24), 8490. <https://doi.org/10.3390/en14248490>.
- Xu, K., Larsen, K., Shao, Y., Zhang, M., Gao, Z. and Moan, T. (2021), “Design and comparative analysis of alternative mooring systems for floating wind turbines in shallow water with emphasis on ultimate limit state design”, *Ocean Eng.*, **219**, 108377. <https://doi.org/10.1016/j.oceaneng.2020.108377>.
- Xue, W. (2016), Design, Numerical Modelling and Analysis of a Spar Floater Supporting the DTU 10MW Wind Turbine (Ph.D. thesis). Norwegian University of Science and Technology, Trondheim, Norway.
- Yang, C.K. and Kim, M.H. (2010), “Transient effects of tendon disconnection of a TLP by hull–tendon–riser coupled dynamic analysis”, *Ocean Eng.*, **37**(8-9), 667-677. <https://doi.org/10.1016/j.oceaneng.2010.01.005>.